




Fiber-coupled superconducting nanowire single-photon detectors integrated with a bandpass filter on the fiber end-face

W J Zhang^{1,2,3} , X Y Yang^{1,2,3}, H Li^{1,2}, L X You^{1,2} , C L Lv^{1,2} , L Zhang^{1,2},
C J Zhang^{1,2}, X Y Liu^{1,2}, Z Wang^{1,2} and X M Xie^{1,2}

¹ State Key Lab of Functional Materials for Informatics, Shanghai Institute of Microsystem and Information Technology (SIMIT), Chinese Academy of Sciences (CAS), 865 Changning Rd., Shanghai, 200050, People's Republic of China

² CAS Center for Excellence in Superconducting Electronics (CENSE), 865 Changning Rd., Shanghai, 200050, People's Republic of China

E-mail: lxyou@mail.sim.ac.cn

Received 14 September 2017, revised 25 December 2017

Accepted for publication 10 January 2018

Published 14 February 2018



Abstract

Superconducting nanowire single-photon detectors (SNSPDs) with both high system detection efficiency (SDE) and low dark count rate (DCR) play significant roles in quantum information processes and various applications. The background dark counts of SNSPDs originate from the room temperature blackbody radiation coupled to the device via a fiber. Therefore, a bandpass filter (BPF) operated at low temperature with minimal insert loss is necessary to suppress the background DCR. Herein, a low-loss BPF integrated on a single-mode fiber end-face was designed, fabricated and verified for the low temperature implement. The fiber end-face BPF was featured with a typical passband width about 40 nm in the 1550 nm telecom band and a peak transmittance of over 0.98. SNSPD with high SDE fabricated on a distributed Bragg reflector was coupled to the BPF. The device with such a BPF showed an SDE of 80% at a DCR of 0.5 Hz, measured at 2.1 K. Compared the same device without a BPF, the DCR was reduced by over 13 dB with an SDE decrease of <3%.

Keywords: superconducting detectors, detection efficiency, dark count rate, bandpass filter, quantum information process

(Some figures may appear in colour only in the online journal)

1. Introduction

Signal-to-noise ratio (SNR) is one of the most important parameters for optical detectors. For single-photon detectors (SPDs), the parameters that determine the SNR are the system detection efficiency (SDE) and the dark count rate (DCR). SPDs that exhibit a high SDE and a low DCR are critical for various quantum and classical optical applications [1–4], such as optical quantum information [1, 2], characterization of quantum emitters [5], and satellite laser ranging [6]. Superconducting nanowire single-photon detectors (SNSPDs) have

shown to be very attractive as SPDs [7–10] because they can provide both high SDE and low DCR, thus surpassing the SDE and DCR of semiconducting avalanche photodetectors [11]. Various applications of high-performance SNSPDs have been demonstrated. For example, a quantum fingerprint beating the classical limit was demonstrated using SNSPDs with an SDE of 45.6% at a DCR of 0.11 Hz [12]. Moreover, quantum key distribution over a 72 dB channel loss was reported using SNSPDs with SDEs of 4%–7% at DCRs of 0.01–0.04 Hz [13]. In 2016, a record 404 km measuring-device-independent quantum key distribution [4] was demonstrated using two SNSPDs with an SDE of 66% at a DCR of 30 Hz.

³ Both authors contributed equally.

Indeed, ideal SPDs should have both near-unity SDE and negligible DCR. To realize the former, one has to ensure that the coupling efficiency, absorption, and intrinsic detection efficiency are as close to 100% as possible. Various results have been reported to that effect [7, 8, 10, 14].

In general, the dark counts of SNSPDs comprise two parts. The first is the intrinsic dark count related to the current-assisted motion of a vortex–antivortex pair [15, 16]. This part of the dark count usually increases logarithmically with the bias current and dominates the DCR when the bias current is close to the switching current. The other is the background dark count caused by the blackbody radiation of the coupling fiber, which plays a key role when the bias current is not close to the switching current. The intrinsic DCR can be neglected in practical applications where the bias current is far from the switching current I_{sw} (e.g., $<0.9 I_{sw}$) and where the SNSPD is operated in the region in which the background DCR is dominant (e.g., below 100 Hz). If an SNSPD with a lower DCR (e.g., 1 Hz or lower) is required, the background dark count has to be suppressed. In addition, the signal photons should not be blocked; i.e., SDE suppression should be avoided. Konstantin *et al* [17] investigated the filtering effect of cooled single-mode optical fibers with varying bending diameters and showed that the minimum DCR can be significantly decreased to 3 Hz with a negligible influence on SDE ($\sim 20\%$). Shibata *et al* [18, 19] reported an ultralow-dark-count SNSPD using a bandpass filter (BPF) and a wavelength-division multiplexer placed in a low-temperature environment but with a 4.5 dB insert loss and a low efficiency of 2.3%. Furthermore, they demonstrated high transmittance using various bulk commercial cold filters [20], but a 2.4 dB loss in SDE still existed. Previously, we reported an SNSPD with a BPF integrated on the back side of the substrate that achieved an SDE of 65% and a DCR of 0.1 Hz [21]. However, this design was limited to SNSPDs with back-side fiber illumination and was therefore incompatible with front-side fiber-illuminated devices such as those that use a distributed Bragg reflector (DBR) [7] or a gold reflector [8] as their cavity structures. In addition, it is impossible to quantify the performance of the filter while it is integrated with the SNSPD.

To realize a universal BPF for fiber coupling and to reduce the insert loss as far as possible, we designed and fabricated a BPF on the end-face of a single-mode fiber (SMF) in the present study. This end-face BPF can easily be aligned with the SNSPD for either front-side or back-side optical coupling. The measured bandpass wavelengths of the BPF are 1540–1579 nm, with the highest transmittance (>0.98 , or <0.08 dB insert loss) at 1567 nm. We fabricated the SNSPD on a DBR substrate and coupled it using the fiber integrated with the end-face BPF. Such a device demonstrated an SDE of 80% with a DCR of 0.5 Hz. Compared with the same SNSPD that uses a normal fiber without a BPF, the DCR of this device was reduced by over 13 dB with an SDE decrease of $<3\%$.

2. Design and characterization of on-fiber BPF

Figure 1(a) depicts the design scheme for the end-face BPF. The BPF comprises non-periodic SiO_2 and TiO_2 bilayers that are alternately deposited layer-by-layer on the end-face of a miniature-unit (MU) SMF. The design of the BPF is based on the interference effect in dielectric multilayer films. The thickness of each SiO_2 (TiO_2) layer usually ranges from zero to one wavelength, which corresponds a light-wave phase change ranging from 0 to 2π . Using the optical-film design software Filmstar, we calculated the transmittance based on the transfer-matrix method and used the genetic algorithm to optimize the precise thickness of each layer. Then, the filter was fabricated by ion-beam assisted deposition (IAD, Optorun OTFC-1300) at a background pressure of 2×10^{-4} Pa. During the process, a mixture of Ar and O_2 was introduced into the system at a working pressure of 2×10^{-2} Pa, and the fiber end-face was heated to roughly 393 K. The deposition rates of TiO_2 and SiO_2 were 0.4 and 0.8 nm s^{-1} , respectively. Direct-transmission monitoring was used to control the thickness of the thin films during the deposition process. The final filter comprised 13 layers, providing a total thickness of approximately $8.8 \mu\text{m}$. The thickness of the SiO_2 layers varied from 264 to 530 nm, whereas the thickness of the TiO_2 layers was fixed at approximately 176 nm. The adhesion and durability of the multilayer thin-film coatings on the fiber connector were quite good. They can withstand multiple fiber wipes without a significant peeling and scratch. In the test of the durability, the samples were encountered cryogenic cycling over ten times, and we did not see any significant changes or degradation in the transmission spectrum.

In figure 1(b), the calculated transmittance of the on-fiber BPF is denoted by the black dashed-dot curve. In the calculation, the refractive indexes used were $n_{\text{TiO}_2} = 2.21$ and $n_{\text{SiO}_2} = 1.46$, which were measured using an infrared ellipsometer. The design passband of the BPF was 1537–1581 nm, with the highest transmittance (from SiO_2 to air) close to 1.0 and a full width at half maximum of 44 nm. The average transmittance for the stopbands (<0.001 (-30 dB)) was in the ranges 1335–1500 nm and 1600–2000 nm. The performance of the end-face BPF was measured at room temperature using a high-precision photometer (Keysight, 81624B), which is indicated by the red curve in figure 1(b). It has a peak transmittance of 0.986 ± 0.005 at a wavelength of 1567 nm, which is higher than that of an on-chip BPF (0.88) [22] and a bulk filter (0.85) [20]. The measured passband is slightly narrower ($\sim 5 \text{ nm}$) than the calculated one, but the central wavelengths are nearly the same. The discrepancy between the calculated and measured filter characteristics may be explained by the imperfect-thickness control and the deviation of the refractive indexes of the film materials. The experimental transmittance of a commercial MU SMF (Thorlabs Inc.) with an anti-refraction coating (ARC) is denoted by the blue curve in figure 1(b), with a peak value of 0.995 ± 0.005 at 1563 nm. The broadband ARC was comprised with multilayers of TiO_2 and MgF_2 , which were deposited by ion-beam sputtering.

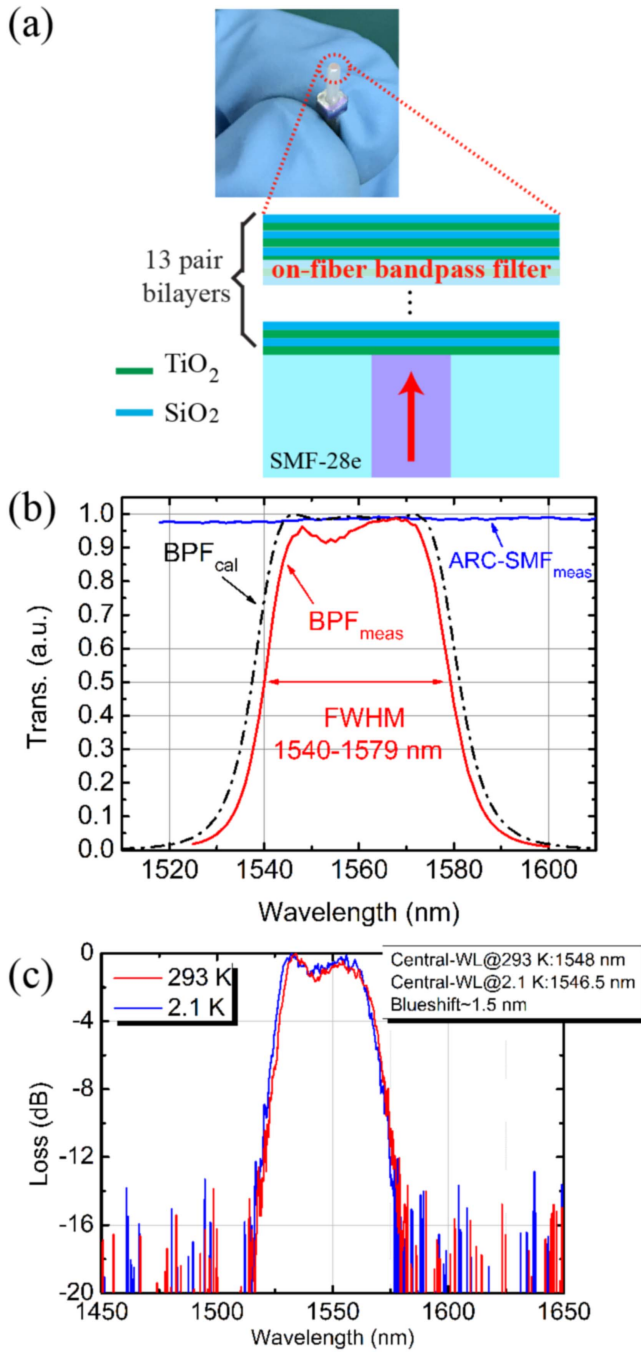


Figure 1. (a) Top: bandpass filter (BPF) integrated on the end-face of a MU single-mode fiber (SMF28e) by ion-beam assisted sputtering; the coating area is pink (indicated by the red dashed circle). Bottom: schematic of the design of the end-face BPF, which comprises 13 pairs of TiO_2 and SiO_2 multi-bilayers. (b) Calculated (BPF_{cal}) and measured (BPF_{meas}) transmittances of the on-fiber BPF as functions of wavelength. The measured results ($\text{ARC-SMF}_{\text{meas}}$) for an SMF with an ARC are also plotted. All data were obtained at room temperature. (c) Temperature dependence of another BPF's passband. The central wavelength measured at 2.1 K has a slight blue-shift (~ 1.5 nm) compared with that measured at 293 K. The measurements were performed for wavelengths of 1450–1650 nm due to limitations of instruments.

Temperature dependence is another important characteristic for BPFs. In our previous work, we used Si and SiO_2 as the dielectric materials for the on-chip BPF [22], which

showed evident temperature dependence because of the low-temperature reflective index changes of Si. The target pass-band was blue-shifted by roughly 20 nm from 300 to 2.9 K. To overcome this effect, we replaced Si with TiO_2 , which has a less temperature-sensitive reflective index [23].

To demonstrate the reproducibility of the performance on the BPF coated fiber, we measured the transmission loss as a function of the wavelength ranging from 1515 to 1600 nm, for six picked-at-random BPF coated fibers fabricated in the same run. Remarkable bandpass features were obtained in all the samples, with a 3 dB cut-off wavelength distribution less than 10 nm. The distribution was due to the slight thickness difference of the deposited dielectric layers between the samples, limited by the fabrication consistency. The averaged central wavelength for the six samples was 1559.7 ± 3.1 nm, close to the designed value of 1559.2 nm. The averaged minimum loss is -0.113 ± 0.075 dB. The best sample (BPF-2#) with a minimum loss of -0.060 dB shown in figure 1(b) was selected and further characterized by coupling with the SNSPD, as shown in the paper.

To verify the temperature dependence of the BPF, we used a homemade setup to measure the transmittance of another BPF as a function of wavelength at various temperatures. The setup involves a commercial tunable laser, an optical power meter, a zirconia sleeve, and a Gifford–McMahon (G–M) cryocooler. First, the MU fiber with the BPF was physically connected and sealed to a MU multimode fiber using a sleeve. The sleeve with the fibers was then heatsinked on the cold plate of the cryocooler. The light transmitted through the BPF fiber was collected by the multimode fiber and monitored using a power meter. Figure 1(c) depicts the transmittance as a function of wavelength measured at both 293 and 2.1 K. It was found that the central wavelength at 2.1 K was slightly blue-shifted (~ 1.5 nm) compared with the one measured at 293 K, indicating the excellent consistency between the room temperature and low temperature. It was noted that, the performance of the BPF shown in figure 1(c) is different with that in figure 1(b) due to difficulty in controlling the film thickness of the multilayers deposited on the fiber tip directly though they were made in the same batch. However, the temperature dependence will not change.

3. Device characterization

Figure 2(a) is a schematic of an SNSPD fabricated on a DBR substrate and front-side coupled using a fiber with an end-face BPF. The multilayer coating forming BPF was deposited on MU connector which is glued with standard SMF28e fiber without any additional optical elements. The distance from the end of the fiber to the device which was about $30 \mu\text{m}$ at room temperature, and approximately reduced to about $20 \mu\text{m}$ at the 2 K due to the thermal contraction of the device package [24]. The spot size on the device was estimated to be less than $11 \mu\text{m}$ in diameter, which was smaller than the active area of device. The device under test is an NbN SNSPD

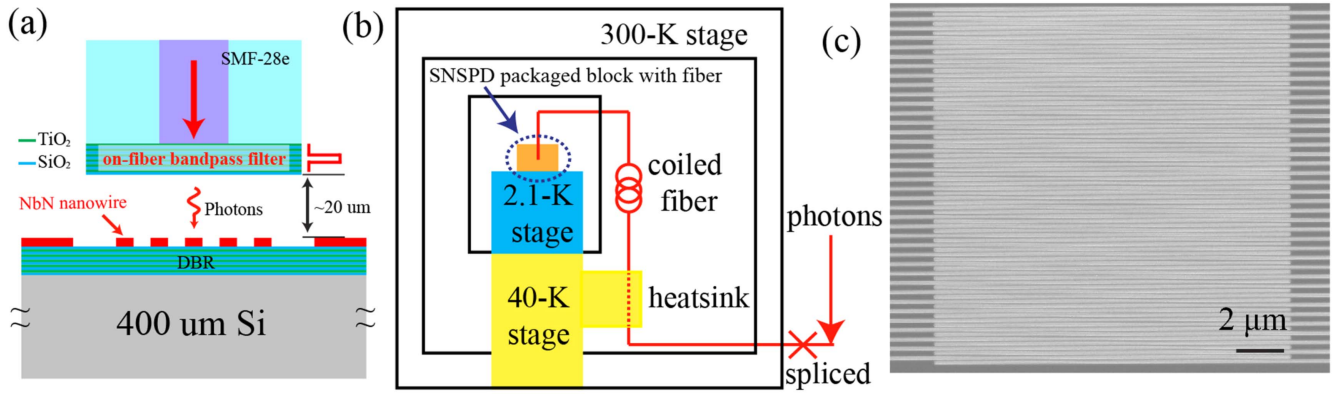


Figure 2. (a) Schematic of a BPF fiber coupled with an SNSPD fabricated on a DBR by front-side illumination. The DBR comprises TiO₂ and SiO₂ multi-bilayers. (b) Schematic of the experimental setup inside the G–M cryocooler. The SNSPD packaged block was mounted on the 2.1 K stage. The fiber (indicated in red) was bent into five turns with diameters of 28 mm and then heatsinked in the 40 K stage. The cold-bent fiber served as a cold filter. (c) Typical scanning electron microscope image of a meander NbN nanowire with an active area of $15 \times 15 \mu\text{m}^2$.

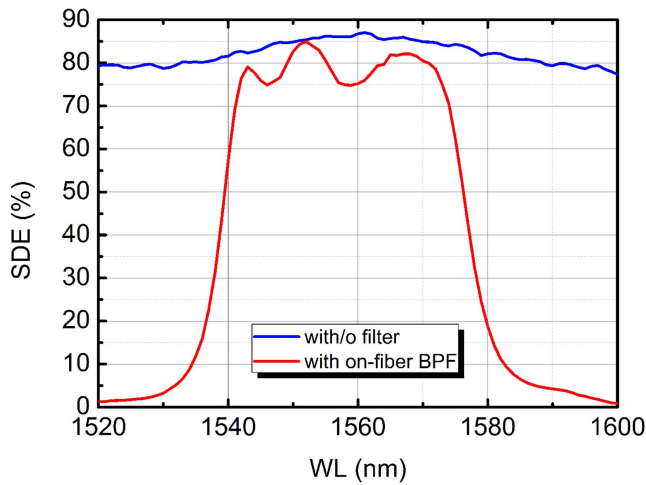


Figure 3. Wavelength dependence of SDE with and without the BPF at a DCR of 100 Hz.

with a nanowire width of 85 nm and a pitch of 160 nm. It covers an active area of $15 \times 15 \mu\text{m}^2$, with a film thickness of roughly 7 nm. The critical temperature and critical current of the device were about 8 K and $10.2 \mu\text{A}$, respectively. The device was fabricated using a process based on electron-beam lithography and reactive-ion etching [7].

To package the BPF fiber with an SNSPD, the BPF fiber was first glued to a copper cap. The cap with the fiber was then aligned with the active area of the device by using an XY-alignment stage and then fixed to the base by screws at room temperature. The alignment error was estimated to be $\pm 3 \mu\text{m}$. The fiber-coupled package was then mounted onto a 2.1 K G–M cryocooler.

Figure 2(b) shows a schematic of the experimental setup inside the cryocooler. The fiber coupled to device was bent into five turns with a diameter of 28 mm to filter the long-wave radiation ($>2 \mu\text{m}$) [17]. The bending loss was measured to be $<0.05 \text{ dB}$. Then, the fiber was heatsinked and cooled by a copper clamp in the 40 K stage. It was found that, the DCRs of the devices coupled with the heatsinked fiber were about

1.5 times less than the ones without a heatsink at the same bias current. In our setup, the fiber lengths from the 300 K chamber to the 40 K stage and 40–2 K stage were about 40 cm and 30 cm, respectively. If the fiber is not heatsinked to the 40 K stage, the temperature of the coiled fiber could be around 120 K assuming a linear temperature gradient. The effect of the cold filter (coiled fiber) will be reduced because of the high temperature if it is not heatsinked. In this paper, all DCRs were recorded in the heatsinked circumstance.

The electrical signal from the device was amplified using a room-temperature amplifier (LNA-650, RF Bay Inc.) and then input to a photon counter or oscilloscope. In the measurement of DCR, to avoid any stray light from the instruments, the input fiber was cut off and shielded by aluminum foil at room temperature (indicated by the red ‘×’ in figure 2(b)). Each DCR data point was collected for 50 s and then averaged. In the measurement of SDE, the light emitted from a continuous-wave source (Keysight 81640, 1520–1630 nm) was attenuated to a photon flux of $N_p \sim 10^5 \text{ s}^{-1}$ through three-cascaded optical tunable attenuators. The input photon flux was calibrated and monitored using a micro-electro-mechanical system optical switch (Thorlabs Inc., OSW12-1310E) and the optical power meter. The input fiber was spliced to the fiber with the BPF on its other end-face, with a splicing loss of $<0.01 \text{ dB}$. The count rate (CR) was collected for 5 s and then averaged. The SDE was calculated using the expression $\text{SDE} = (\text{CR} - \text{DCR})/N_p$, including all the system optical loss. The relative uncertainty of the SDE values was estimated to be $<3\%$.

4. Performance of SNSPDs with and without BPF

The SDE and DCR were systematically measured for the SNSPD coupled with the BPF fiber. For comparison, we also measured the same SNSPD coupled with a conventional ARC-lens SMF with a beam waist of $7 \mu\text{m}$ and a device–fiber distance of roughly $185 \mu\text{m}$. The lens SMF was used to reduce the beam waist at a distance from the end of the fiber,

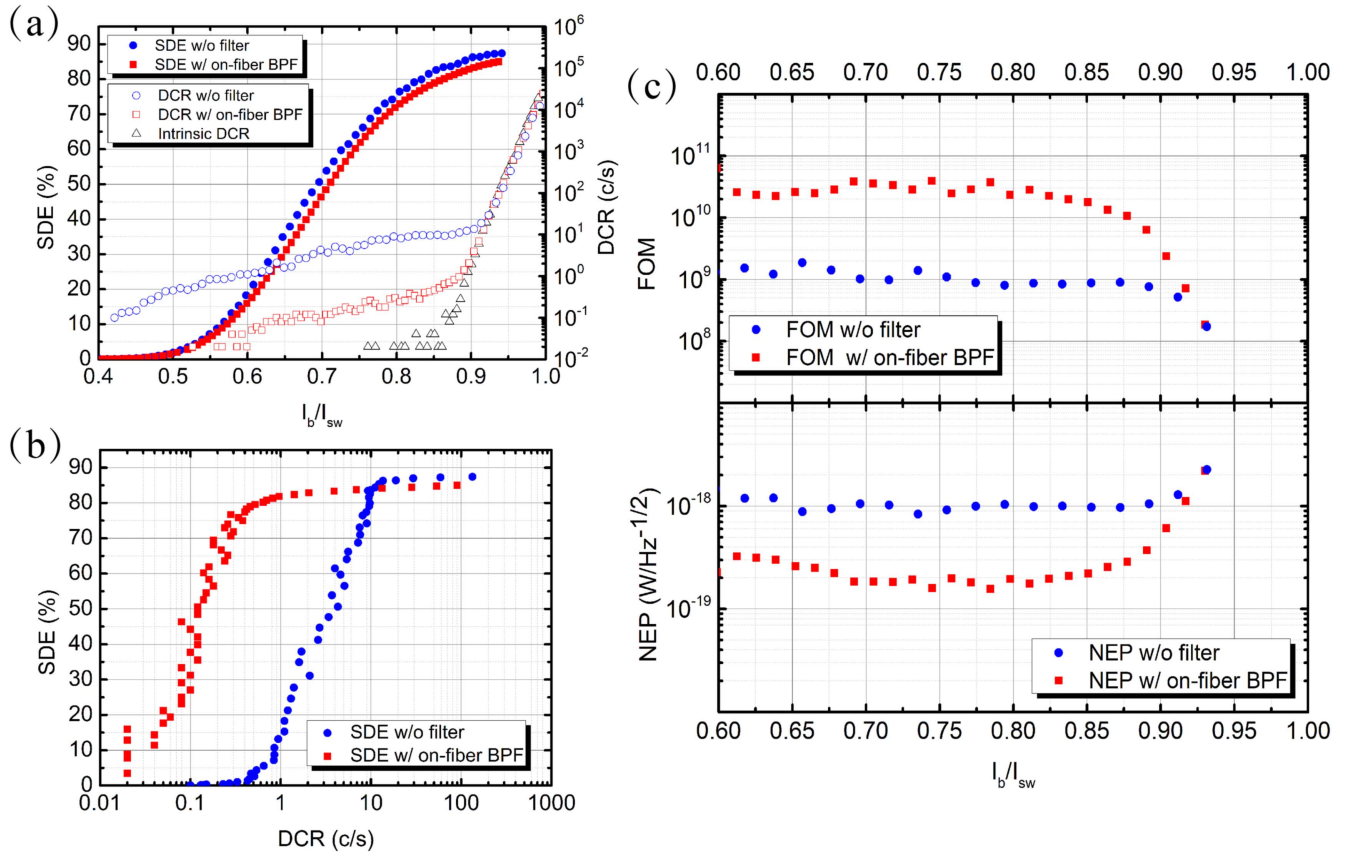


Figure 4. (a) Normalized bias-current dependence of SDE and DCR for an SNSPD coupled using a fiber with and without a BPF on its end-face. The intrinsic DCR of the device is also plotted. (b) SDE as a function of DCR without (blue dots) and with (red squares) a BPF. (c) Top: figure of merit (FOM). Bottom: noise equivalent power (NEP) as a function of bias current for devices with/without end-face BPF.

Table 1. Details for SNSPDs used in the reproducibility measurement. The nanowire width and pitch were 85 and 160 nm for all the SNSPDs.

SNSPD	Material	Thickness (nm)	Active area (μm^2)	SDE _{max} (%)		f_E		I_{sw} (μA)
				w/o BPF	w/BPF	NEP	FOM	
D9 ^a	NbN	7	15*15	87	85	5.3	28.8	10.2
C5	NbN	7	18*18	84	84	3.5	11.3	9.6
F6	NbTiN	5	18*18	84	82	3.6	13.9	12.2
G4	NbTiN	5	15*15	81	82	4.4	18.7	14.3

^a The data of the device (D9) was shown in figure 4. f_E denotes the enhanced factor of NEP (FOM) determined at $0.8I_b/I_{sw}$ for each device coupled with the BPF, in contrast to the case without BPF.

where the small-gradient index lenses were directly fusion spliced to the end of SMF28e. More details can be found in [25].

Figure 3 depicts the wavelength dependence of the SDE of the SNSPD with and without a filter. Notably, figures 1(b) and 3 were the results for the same BPF fiber. The data were recorded at a normalized bias current of 0.94 ($9.6 \mu A$) with a DCR of 100 Hz in both cases. The maximum SDEs with and without a BPF were 85% at 1551 nm and 87% at 1562 nm, respectively. The SDE with a BPF was slightly less than that without a BPF because of a difference in the coupling efficiency. Without the BPF, the SDE showed a broad resonant band around 1550 nm with small periodic fringes that can be attributed to light interference between the fiber end-face and

the device surface [26]. In contrast, for the case with a filter, the SDE demonstrated a prominent BPF effect, with a profile similar to the transmittance data shown in figure 1(b). In detail, the maximum change in efficiency shown in figure 3, is $75\%/85\% \approx 0.88$ for the two cases at the wavelength of about 1560 nm. This value is slightly smaller than the local minimum of the transmission in the middle of the filter with a value of 0.91 in figure 1(b). The wavelength dependence of the SDE demonstrates the proper functioning of the on-fiber BPF. The SDE fringes of the passband were different from the interference patterns caused by optical path difference between the fiber tip and the device [26], since the first dip was caused by the imperfect BPF shown as figures 1(b) and (c) instead of the interference. As a result, we can not use the

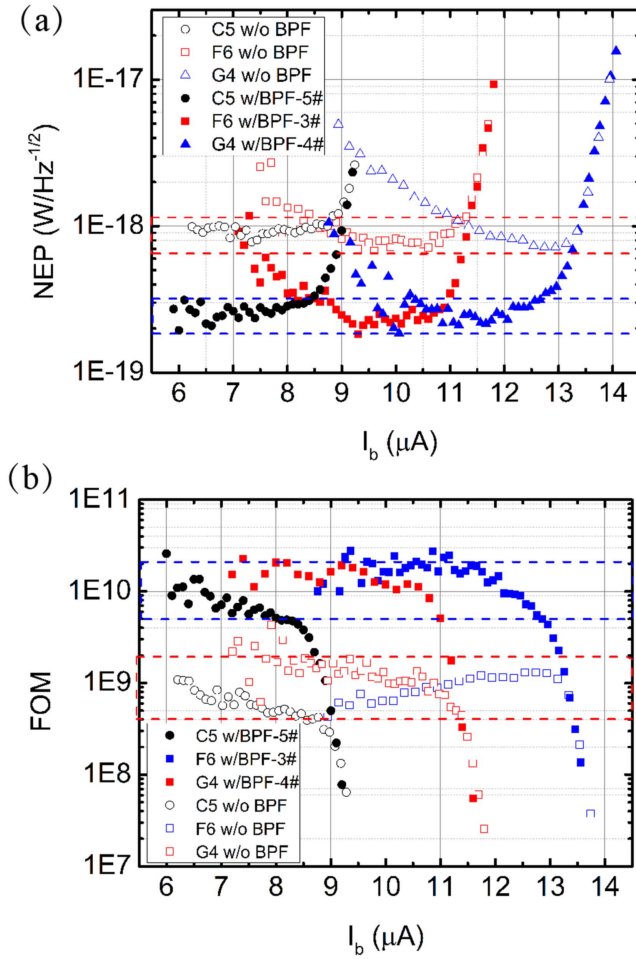


Figure 5. Comparison of NEP (a) and FOM (b) for three different SNSPDs with and without the BPF fiber coupled (C5, F6 and G4).

feature to calculate the distance between the fiber and the device. The existence of fringes could result in an unwanted maximal SDE shift from the target wavelength, if the device–fiber distance was not in a good control. In future, this unwanted wavelength shift can be reduced by either fine controlling the device–fiber distance or fabricating an ARC layer on the device surface.

The temperature insensitivity of the BPF can also be verified by recording the wavelength dependence of the SDE for SNSPDs coupled with the BPF coated fiber. For example, in figure 3, the central wavelength of 1558 nm indicated a slight blue-shift less than 2 nm, in contrast to the transmitted data measured at 300 K showed in figure 1(b). This result was consistent with the measurement results showed in figure 1(c).

Figure 4(a) summarizes the SDE, DCR, and intrinsic DCR as functions of the normalized bias current for an SNSPD with or without a BPF on the fiber end-face. The SDEs were measured at their maximum values shown in figure 3, namely at 1551 nm (with BPF) and 1562 nm (without BPF). The intrinsic DCR was recorded with the device shielded in a copper box with no connected fiber and was cooled to 2.1 K. The intrinsic DCR dominates in both cases for normalized bias currents >0.9 , and deviations

occurred at lower bias currents ($\sim 0.9 I_{\text{sw}}$) because of the different contributions of the background dark counts. The deviation appears at a different inflection point in either case. The inflection point of the DCR without a BPF was roughly 13 Hz, whereas the one with a BPF was reduced by over an order of magnitude to about 1 Hz.

To further establish a straightforward comparison of performance for practical applications, the DCR dependence of SDE with or without a BPF is shown in figure 4(b). At DCRs of 10 Hz and higher, both the SDE values were roughly 85%. At a fixed SDE of 80%, the DCRs were 0.5 Hz (with BPF) and 10 Hz (without BPF), namely a ratio of 20, i.e., over 13 dB.

To quantitatively evaluate the performance of an SNSPD with or without a BPF, two parameters were introduced. One is the figure of merit (FOM) [5] defined as $\frac{\text{SDE}}{\text{DCR} \times T_j}$, and the other is the noise equivalent power (NEP) defined as $\frac{h\nu \times \sqrt{2 \times \text{DCR}}}{\text{SDE}}$, where T_j is the timing jitter of the system. The timing jitter T_j with or without a BPF was measured as a function of the bias current using a reported [9] femtosecond laser at 1550 nm and a time-correlated single-photon counting module in the single-photon limit. By comparing T_j values at the same bias current, we found that the integrated BPF exerted negligible influence on the timing jitter. Typically, the measured T_j was at a value of 83 ps at a normalized bias current of 0.94 (9.6 μA). As shown in figure 4(c), the best FOM and NEP of the device with a BPF reached 3.7×10^{10} and $1.6 \times 10^{-19} \text{ W/Hz}^{-1/2}$ at a DCR of 0.3 Hz and an SDE of 73%. It was found that, the improvement on FOM (NEP) was significant, which is about 20–30 times (5–6 times) in contrast to the ones without BPF. Clearly, using an on-fiber BPF can effectively suppress the DCR without sacrificing SDE, thereby providing an excellent solution for various applications that require both high SDE and low DCR.

5. Performance reproducibility of SNSPDs coupled with the BPF coated fiber

To further demonstrate of the reproducibility of the performance on the BPF coated fiber, the fibers were coupled to the several SNSPDs and characterized at 2.1 K. No significant changes in performance of the BPF coated fibers were found after the first measurement nearly a year ago. Then, the durability of the BPF coated fibers was confirmed. The details were shown in table 1. The devices with a larger active area of $18 \times 18 \mu\text{m}^2$ were introduced to study the influence of the coupling efficiency. Also, no notable difference was found in the SDEs between the devices with different active areas ($15 \times 15 \mu\text{m}^2$ and $18 \times 18 \mu\text{m}^2$), indicating a reliable optical coupling.

Figure 5 showed the comparisons of the NEP and FOM for fiber-coupled SNSPDs with or without the BPF, where DCR and T_j is the DCR and the timing jitter of the device, respectively. Since the difference in the SDEs was quite small, the difference of NEP or FOM is mainly contributed by DCR. For the devices coupled to SMF without the BPF (with

BPF coated fiber), their NEPs fell into a plateau region of $7\text{--}10 \times 10^{-18}$ ($1\text{--}3 \times 10^{-19}$) $\text{W Hz}^{-1/2}$, indicated with red (blue)-dashed squares. Correspondingly, the FOMs of the devices coupled to SMF without the BPF (with BPF coated fiber), were distributed in a plateau region of $4\text{--}20 \times 10^8$ ($5\text{--}20 \times 10^9$). The enhanced factor f_E of NEP (FOM) determined at $0.8I_b/I_{sw}$ for each device was listed in table 1, indicating that the performance of the devices coupled with a BPF coated fiber were improved.

6. Discussion

Our experimental results show that the on-fiber BPF is functional and performs better than existing solutions. However, several issues must be solved before the performance can improve, such as reducing the deviation between design and fabrication, improving the thickness control, and studying the variance of refractive index in the deposition process. To reduce the interference between the fiber end-face and the device surface, one could design a BPF integrated on a lens fiber with a long focal distance. To further suppress the background dark count, one could reduce the bandwidth of the BPF.

7. Conclusion

In conclusion, to suppress the background DCR in an SNSPD, we designed, fabricated and measured a low-loss BPF on the end-face of an SMF, with a bandwidth of roughly 40 nm and a maximum transmittance of over 0.98 at 1567 nm. The temperature dependence of the bandpass wavelengths showed a blue-shift of roughly 1.5 nm at 2.1 K compared with that at room temperature. This negligible blue-shift was facilitated using temperature-insensitive materials, namely SiO_2 and TiO_2 . As a demonstration, an NbN SNSPD was front-side coupled to an SMF with or without an end-face BPF. The experimental results showed that, with an end-face BPF, the SDE reached a maximum of 80% and the DCR was reduced by over 13 dB to 0.5 Hz. Such a high SDE/low DCR SNSPD with an on-fiber BPF would be immediately suited to quantum key distribution and other applications. In addition, fibers with end-face BPFs could be commercialized independently, thereby representing an interesting accessory to SNSPDs and other applications of SPDs.

Acknowledgments

This work is supported by National Key R&D Program of China (2017YFA0304000), the Science and Technology Commission of Shanghai Municipality under Grant (16JC1400402), the National Natural Science Foundation of China (NSFC) (61401441, 61501439, and 61401443).

ORCID iDs

W J Zhang  <https://orcid.org/0000-0002-9432-7404>

L X You  <https://orcid.org/0000-0001-7304-0474>

C L Lv  <https://orcid.org/0000-0003-4343-4071>

References

- [1] Takesue H *et al* 2007 Quantum key distribution over a 40 dB channel loss using superconducting single-photon detectors *Nat. Photon.* **1** 343
- [2] Sun Q-C *et al* 2016 Quantum teleportation with independent sources and prior entanglement distribution over a network *Nat. Photon.* **10** 671
- [3] Liu Y *et al* 2016 Experimental quantum data locking *Phys. Rev. A* **94** 020301
- [4] Yin H-L *et al* 2016 Measurement-device-independent quantum key distribution over a 404 km optical fiber *Phys. Rev. Lett.* **117** 190501
- [5] Hadfield R H 2009 Single-photon detectors for optical quantum information applications *Nat. Photon.* **3** 696
- [6] Li H *et al* 2016 Superconducting nanowire single photon detector at 532 nm and demonstration in satellite laser ranging *Opt. Express* **24** 3535
- [7] Zhang W J *et al* 2017 NbN superconducting nanowire single photon detector with efficiency over 90% at 1550 nm wavelength operational at compact cryocooler temperature *Sci. China Phys., Mech. Astron.* **60** 120314
- [8] Marsili F *et al* 2013 Detecting single infrared photons with 93% system efficiency *Nat. Photon.* **7** 210
- [9] You L X *et al* 2013 Jitter analysis of a superconducting nanowire single photon detector *AIP Adv.* **3** 072135
- [10] Rosenberg D, Kerman A J, Molnar R J and Dauler E A 2013 High-speed and high-efficiency superconducting nanowire single photon detector array *Opt. Express* **21** 1440
- [11] Zhang J, Itzler M A, Zbinden H and Pan J-W 2015 Advances in InGaAs/InP single-photon detector systems for quantum communication *Light Sci. Appl.* **4** e286
- [12] Guan J-Y *et al* 2016 Observation of quantum fingerprinting beating the classical limit *Phys. Rev. Lett.* **116** 240502
- [13] Shibata H, Honjo T and Shimizu K 2014 Quantum key distribution over a 72 dB channel loss using ultralow dark count superconducting single-photon detectors *Opt. Lett.* **39** 5078
- [14] Miki S, Yamashita T, Terai H and Wang Z 2013 High performance fiber-coupled NbTiN superconducting nanowire single photon detectors with Gifford-McMahon cryocooler *Opt. Express* **21** 10208
- [15] Yamashita T *et al* 2011 Origin of intrinsic dark count in superconducting nanowire single-photon detectors *Appl. Phys. Lett.* **99** 161105
- [16] Bartolf H *et al* 2010 Current-assisted thermally activated flux liberation in ultrathin nanopatterned NbN superconducting meander structures *Phys. Rev. B* **81** 024502
- [17] Konstantin S *et al* 2015 Dependence of dark count rates in superconducting single photon detectors on the filtering effect of standard single mode optical fibers *Appl. Phys. Express* **8** 022501
- [18] Shibata H, Shimizu K, Takesue H and Tokura Y 2013 Superconducting nanowire single-photon detector with ultralow dark count rate using cold optical filters *Appl. Phys. Express* **6** 072801
- [19] Shibata H, Shimizu K, Takesue H and Tokura Y 2015 Ultimate low system dark-count rate for superconducting nanowire single-photon detector *Opt. Lett.* **40** 3428

- [20] Shibata H *et al* 2017 SNSPD with ultimate low system dark count rate using various cold filters *IEEE Trans. Appl. Supercond.* **27** 1
- [21] Yang X Y *et al* 2014 Superconducting nanowire single photon detector with on-chip bandpass filter *Opt. Express* **22** 16267
- [22] Yang X Y *et al* 2015 Temperature dependence of an optical narrow-bandpass filter at 1.5 μm *Appl. Opt.* **54** 96
- [23] Chu A K, Lin H C and Cheng W H 1997 Temperature dependence of refractive index of Ta₂O₅ dielectric films *J. Electron. Mater.* **26** 889
- [24] Dengkuan L *et al* 2013 Fiber coupling of superconducting nanowire single-photon detector *Opt. Precis. Eng.* **21** 1496
- [25] Miki S *et al* 2011 Characterization of coupling efficiency and absorption coefficient for fiber-coupled SNSPD with an optical cavity *IEEE Trans. Appl. Supercond.* **21** 332
- [26] Lita A E, Miller A J and Nam S W 2008 Counting near-infrared single-photons with 95% efficiency *Opt. Express* **16** 3032